Hybrid Passivation for Foldable Indium Gallium Zinc Oxide Thin-Film Transistors Mediated by Low Temperature and Low Damage Parylene-C/ALD-AlOx Coating

Shijie Zhan, Soodeok Han, Sang Yun Bang, Benxuan Li, Young Tea Chun, Bo Hou and Jong Min Kim*

Engineering Department, University of Cambridge, 9 JJ Thomson Avenue, Cambridge CB3 0FA, UK University of Cambridge, CB3 0FA, Cambridge, UK

*Corresponding author. Tel: +44 (0)1223 748318. Email: bh478@cam.ac.uk (Bo Hou)

Keywords: IGZO TFT, Hybrid Passivation, Bias Stability, Mott-Schottky Plot, TFT Matrix

Abstract

Indium gallium zinc oxide (IGZO) thin-film transistors (TFTs) are primary components in integrated active electronics. Due to the multiple layers' deposition and integration, the development of prevalent active integrated electronics such as flat-panel displays, sensor arrays, and flexible circuitry heavily depends on high-throughput passivation techniques. Though oxide compound semiconductors are commonly used for providing uniform and robust passivation, it usually causes performance degradation on IGZO TFTs during passivation process. Herein, a Parylene-C/AlO_x hybrid passivation approach has been introduced to reduce the damage during AlO_x atomic layer deposition (ALD), which results in high-performance depletion-mode IGZO TFT to be fabricated on polyethylene naphthalate (PEN) substrate with enhanced bias stability. Compared with Parylene-C passivation, the hybrid passivated IGZO TFTs exhibit excellent saturation mobility (7.9 cm^2/Vs), ON/OFF ratio (10^7), hysteresis window (0.73V) and bias stability (1.44V and -0.27V threshold voltage shift, V_{ds}=20V). Based on systematic Mott–Schottky and X-ray diffraction characterisations, we found TFT performance enhancement are originated from their doping density variation which resulted from a Parylene-C/ALD-AlO_x microstructural hybridisation. Finally, this method has be implemented to wafer-scale integrated circuits with high uniformity and a flexible 10×10 IGZO TFT backplane matrix on a PEN substrate (2.5cm×2.5cm).

1. Introduction

Amorphous oxide thin-film transistors (TFTs), especially indium gallium zinc oxide (IGZO) TFTs are primary components in modern large-area active electronics, especially in display backplane technologies due to their higher channel mobility, robust processability and larger ON/OFF ratio compared to the conventional amorphous silicon TFTs [1-7]. In general, additional passivation layers need to be deposited to protect TFT channels from potential physical damage during subsequentially multiple-layer integration processes [6, 8, 9]. Moreover, these passivation layers can also enhance the device stability of TFTs, achieving enhanced bias stability, small hysteresis and stable ON/OFF ratio, via suppressing the diffusion of oxygen and water molecules to the channel layers [10, 11]. For instance, oxide materials, such as AlO_x, SiO_x, TiO_x and HfO_x are widely used as passivation layers because of their small lattice mismatch between IGZO, and low oxygen and water permeability [1, 12-17]. However, performance degradation of IGZO TFTs has been commonly observed after the deposition of oxide passivation layers, regardless of their deposition techniques such as Plasma-Enhanced Chemical Vapor Deposition (PECVD), Atomic Layer Deposition (ALD) or sputtering deposition process [12, 18]. These damaged channels are subjected to poor bias stability and even loss of modulation. High-temperature annealing (above 300 °C) may alleviate the degeneration [18-20]; however, this thermal treatment process is not suitable for the development of emerging flexible and foldable plastic electronics [1, 21, 22]. As an alternative, polymers such as SU-8, Polydimethylsiloxane (PDMS), CYTOP and Parylene have been adopted to passivate TFT channels associated with their relatively mild deposition condition [19, 23-26]. However, polymers typically have high oxygen and water permeability, and may also not be resistive to some solvents during following integration processes, which make polymers not sufficient to passivate IGZO TFTs [11, 27].

Recently, people have developed a bilayer passivation approach to combine both organic layers as a buffer layer and oxide semiconductors. For instance, Teflon/sputtered-SiO_x bilayer passivation structure has been proposed to mitigate the impairment from the sputtering process, which results in considerable enhancement of the TFT reliability [28]. Moreover, a Parylene/AlO_x bilayer passivation with sputtered AlO_x has been designed to keep Parylene from bombardment damage during sputtering process, which has achieved excellent IGZO TFT bias stability with ~2.5 V V_{th} shift after 3600 s positive stress (1uA) [29]. However, the bias stability achieved by these

bilayer passivation methods is still inferior compared to the TFTs passivated only by sputtered AlO_x [30]. One promising way is to deposit AlO_x by ALD instead of sputtering because of its enhanced coating conformity, higher film density and lower damage from the ALD process. Furthermore, the conformal ALD coating of AlO_x may infill into the pinholes and voids in Parylene films and block the water/oxygen penetration paths, which is beneficial to the bias stability of IGZO TFTs. Besides, compared with the ambient sputtering deposition, ALD with slightly elevated deposition temperature (~120 °C) can also facilitate the re-crystallisation of Parylene-C and may result in a self-assembled hybrid structure between Parylene-C and AlO_x.

In this work, we propose an ALD-enabled hybrid Parylene-C/AlO_x structure for passivating the IGZO TFT channels with excellent bias stability. Through a sequential deposition of Parylene-C and ALD grown AlO_x, we find a hybrid passivation approach can not only eliminate the physical deposition damages but also blocks water/oxygen penetration paths. We show the bias stability of hybrid passivated IGZO TFTs is much better than the Parylene-C only counterpart. Mott-Schottky analysis and XRD diffractogram reveal the performance and stability improvement are originated from a formation of hybrid structure between Parylene-C and ALD-AlO_x. Finally, to show the potential of using this hybrid passivation method for flexible integrated-electronics, an IGZO TFT matrix array passivated by Parylene-C/ALD-AlO_x hybrids was fabricated, and the uniformity data of as-prepared TFTs is demonstrated.

2. Experimental Procedure

The single-pixel IGZO TFTs were fabricated on doped *p*-type Si wafers with a thermally grown 200 nm SiO_2 dielectric layer. The channels were passivated by Parylene-C, AlO_x or hybrid structure, and top contacts are Ti/Al. Typically, SiO_2 (200 nm)/*p*-Si wafers were thoroughly cleaned with acetone and isopropyl alcohol (IPA) in a sonication bath for 10 minutes, and then dried by N_2. Amorphous IGZO (In_2O_3: Ga_2O_3: ZnO = 2:1:2 at weight percentage) was deposited on the cleaned substrates through RF sputtering. In the sputtering process, RF power, Ar flow, chamber pressure, substrate temperature and film thickness were fixed at 75 W, 25 sccm, 6.5 mtorr, room temperature and 30 nm, respectively. Then IGZO films were patterned through wet etching using 1% HCl solution in DI water. A top contact of 10 nm Ti/100 nm Al was deposited by an e-beam evaporator after the photolithography process. Afterwards, the

devices were baked at 150 ºC for 1 hour under an ambient condition. To deposit the hybrid structure, 200 nm Parylene-C was coated on TFTs by a Parylene coater with chamber temperature at room temperature; then a 50 nm AlO_x layer was deposited at 120 ℃ using a Savannah ALD system. The reference samples include TFTs without passivation, with 200 nm Parylene-C passivation and with 50 nm ALD-AlO_x passivation were prepared separately using the same preparation procedures.

Corning glass and PEN are selected as transparent substrates for the hybrid passivated TFT backplane matrices fabrication. Typically, gate layers of 10 nm Ti/100 nm Al were deposited by an e-beam evaporator after the photolithography process on corning glasses or PEN substrates. Instead of SiO_2, a 50 nm-HfO_x was deposited by ALD at 150 ℃ as the dielectric layer. Following steps for the deposition of top contact and the hybrid passivation were similar to the procedures as mentioned in the single-pixel devices.

The electrical characterisation of all TFTs was carried out by SCS 4200 Keithley semiconductor analyser in ambient with the temperature at 24.8 ℃ and relative humidity at 43%. For the transfer characteristics, drain voltage is biased at 20V with gate voltage scanned from -5V to 20V. In bias stability tests, gate voltage was set to 10V/-10V for positive- bias-stress (PBS)/ negative-bias-stress (NBS) test and drain voltage was set to 20 V for both conditions. The scan time was set at 0 s, 100 s, 200 s, 400 s, 600 s, 900 s, 1800 s, 2700 s, 3600 s with the stress condition mentioned above. The Mott-Schottky analysis was taken on the structure Si/SiO_2 (200 nm)/ IGZO (30 nm)/ Ti (10 nm)/ Al (100 nm) with the frequency at 1k Hz and scan delay of 0.05 s.

3. Results and discussion

The IGZO TFTs are fabricated following the typical thin film deposition and integration procedures. The hybrid passivation strategy and corresponding device cross-section diagram are shown in Fig.1 where the grey zigzag and white parts in the Parylene-C film represent pinholes and voids, which can facilitate oxygen and water penetration. During the ALD process, AlO_x precursors may infill into the pinholes and in situ growth AlO_x inside of these voids, therefore, enables low density of pinholes and voids via hybrid passivation.

Transfer curves and extracted parameters from the unpassivated IGZO TFT and TFTs

with different passivation are shown in Fig.2. With the direct coating of AlO_x on an IGZO channel through ALD, the TFT becomes too conductive to work as a transistor and cannot be switched off with -5V gate bias while the original unpassivated TFT has proper transfer characteristics. As a solution to this issue, the hybrid passivation, consisting of 200 nm Parylene-C as a buffer layer between IGZO channel and AlO_x, remarkably improved TFT modulation performance compared with the AlO_x passivated one. From the extracted parameters, we found the hybrid passivation structure can successfully preserve TFT saturation mobility ~8 cm^2/Vs and ON/OFF ratio ~10^8 comparable to the Parylene-C passivated one. Moreover, due to the AlO_x passivation, the hybrid structure enables TFTs to have smaller V_{th} (2.9 V) than Parylene-C passivated TFT (5.2 V), which allows lower working voltage and thus lower power consumption.

As shown in Fig.2(b), the hybrid passivation helps narrow the hysteresis window. Compared to the large hysteresis window of 1.46 V in the Parylene-C passivated TFT, the hysteresis window in the hybrid layer passivated one is only 0.73 V. Indeed, the previous report has proposed that oxygen adsorption under positive gate bias can induce V_{th} right-shift which may cause a clockwise hysteresis between forward and back scan [10]. Therefore, it can be inferred that the hybrid passivation has a better ability to prevent oxygen from getting into the channel compared to the Parylene-C passivation. Besides, the intrinsic electric dipole in AlO_x may also contribute to the reduced hysteresis in the hybrid layer passivated TFT, because electric diploes in an AlO_x passivation layer can offset the clockwise hysteresis in IGZO TFTs [31].

In addition to the narrower hysteresis window, the Parylene-C/AlO_x hybrid passivation also features excellent bias stability. The devices were stressed under conditions with drain voltage at 20 V and gate voltage at 10 V/-10 V for positive and negative stress so that the drain current was larger than 50 uA. It is a severe stress condition considering the fact that in AMOLED display 1uA is usually required to drive pixels [32]. In Fig 3, it is shown that Parylene-C passivation only slightly reduces the PBS V_{th} shift from 6.12 V to 4.10 V within 3600 s stress time while the hybrid passivated IGZO TFT has much smaller PBS V_{th} shift of only 1.41 V. The increased V_{th} after positive gate bias is originated from the oxygen molecule adsorption and water molecule desorption at the channel surface, which depleted the electron channel in the IGZO film. For the negative bias condition, an unexpected positive V_{th} in unpassivated IGZO TFT is observed,

where usually a reverse process of molecule adsorption to the positive bias condition causes accumulated electrons and thus a negative V_{th}. However, it is worth noting that a hump effect occurs in both unpassivated and Parylene-C passivated TFT samples in Fig.3(b)(d). The water molecule adsorbs onto the channel surface and even diffuses into the channel as defects, which is regarded as the cause of the hump effect [31]. Therefore, when water molecules form traps in the IGZO channel, the V_{th} will be raised to compensate the negative shift of V_{th} in the NBS condition and make the total V_{th} close to zero. After passivating the channel with Parylene-C, the water molecule, however, can still penetrate and stay in the voids and pinholes of the Parylene-C film, but it has lower chances to diffuse into the IGZO channels. Therefore, the effect of water adsorption is stronger than the effect of water molecule diffusion, which makes the negative bias stability (V_{th} -1.26 V) even worse compared to the original TFT. With the hybrid passivation, the hump effect has been eliminated, and water molecule adsorption is effectively suppressed (V_{th} shift ~ -0.27 V). Therefore, it can be seen that the hybrid passivation has superior passivation performance with lower oxygen and water permeability than the Parylene-C passivation.

To investigate the mechanism of transfer characteristic variation and bias stability improvement after hybrid passivation on the IGZO channel, Mott–Schottky analysis was conducted. As shown in Fig.4, the electron concentration from IGZO channels with different passivation can be extracted according to the Mott-Schottky equation [33]:

$$C^{-2} = \frac{2}{\epsilon_s A^2 e N_D}\left(V - V_{fb} - \frac{k_B T}{e}\right)$$

Here, C and A are the capacitance and area size of the semiconductor/insulator interface. ϵ_s and e is the semiconductor permittivity and elementary electrical charge constant. k_B and T are the Boltzmann's constant and the absolute temperature. V and V_{fb} are the voltage applied on the junction and the flat band voltage. N_D is the donor concentration of the semiconductor. With the equation, a straight line can be found in the plot of $1/C^2$ against V, in which N_D can be calculated:

$$\frac{\partial C^{-2}}{\partial V} = \frac{2}{q A^2 \epsilon_s N_D}$$

In our work, Mott–Schottky analysis was taken using the structure of Si/SiO_2/IGZO/Ti-Al. Since electrons in n-type oxide semiconductors come from the oxygen vacancy,

donor concentration N_D in IGZO is equal to the electron concentration. The electron concentration is calculated from the dotted straight lines in Fig.4(a)~(c). Consistent with the left shift of transfer curve from Parylene-C passivated TFT to the hybrid layer passivated TFT in Fig.2(a), the effective carrier concentration of hybrid layer passivated IGZO is $4.74*10^{21}$ cm^{-3}, larger than $4.16*10^{21}$ cm^{-3} of Parylene-C passivated IGZO. The larger carrier concentration in the hybrid layer passivated TFT also accounts for the higher off-current compared with the Parylene-C passivated TFT. And the conductive transfer curve of AlO_x passivated TFT can be explained by the high electron concentration at $7.7*10^{24}$ cm^{-3}, which is too high to be depleted with -5 V gate bias. Moreover, the electron concentration of the IGZO channel after holding the bias for 600 s was extracted and compared with the initial electron density in Fig.4(d). The smaller variation of carrier concentration after 600s bias stress in the hybrid passivated IGZO channel compared to the Parylene-C passivated one indicates enhanced bias stability with hybrid passivation. From Mott–Schottky analysis, it is found that the passivation changes the transfer characteristics of an IGZO TFT by controlling the "doping" level of the channel. Variation of electron concentration caused by adsorption of oxygen and water as well as the damaging effect from ALD-AlO_x can be well suppressed by hybrid passivation.

Based on systematic X-ray diffraction analysis, we found the advantages of hybrid passivation structure don't just come from a simple superposition of the Parylene-C and AlO_x layer in the vertical direction. From the XRD pattern and the fitted peaks shown in Fig.5(a), the Parylene-C film has a board peak at 13.6° for (020) crystallographic plane and a more board peak in the range of 20°~40° (maxima around 22.8°) for the amorphous parts [34]. The AlO_x only exhibits a board peak around 24.4°, which slightly shows the orientation of (012) facet with the amorphous background. It should be noticed that a sharp and strong peak occurs in the hybrid film which locates very close to the (020) peak of the Parylene film but is slightly right-shifted from 13.6° to 14.1°. With the coating of AlO_x, the width of the (020) peak from Parylene-C becomes much smaller, which indicates a potential recrystallisation process of the Parylene film during the 120 °C ALD process. For the amorphous XRD pattern between 20° and 40°, the hybrid film shows a board peak with the maxima ~23.2°, which is located between the amorphous peak of Parylene-C at around 22.8° and the board peak of AlO_x around 24.4°. The XRD peak of the hybrid structure isn't direct composition of the peaks from

the Parylene-C and AlO_x, but a compromise in between, inferring a potential hybrid structure formed by ALD-AlO_x and Parylene-C [35]. Fig.5(b) exhibits the schematic of the hybrid structure built from Parylene-C and AlO_x. During the ALD process, the conformal coating allows the AlO_x to be deposited within the gaps among the Parylene-C chain instead of just coating on top of it. Being coated with amorphous AlO_x, the amorphous hybrid structure varies which changes the location of its XRD peak. Since the penetration paths within the hybrid structure are blocked, there is little diffusion path left for oxygen and water molecule, which provides the hybrid layer passivated IGZO TFTs with excellent bias stability. This hybridisation process is one of the primary advantages of using ALD to deposit AlO_x instead other methods like sputtering and evaporation due to its excellent conformity.

With the ALD coating for AlO_x, the surface roughness reduces considerably according to the AFM data in Fig.6. There is a significant fluctuation at the surface of Parylene-C with deep and broad 'valleys' at the dark area while the 'valleys' are smaller and shallower at the surface of the hybrid film, as shown in the two 3D mapping images. As the distribution of surface height shows in Fig.6(b)(d), the surface roughness reduces from ~10 nm for the Parylene-C film to ~4 nm for the hybrid film, which implies the function of ALD AlO_x to cover the voids and valleys on the surface. This enhancement of surface roughness comes from the coating conformity of the ALD process. A smooth surface is preferred in the following integration processes such as display backplanes where a rough passivation surface may cause non-uniform additional layers deposition.

To demonstrate this Parylene-C/AlO_x hybrid coating method as a promising passivation technique for large-area applications such as display backplanes, uniform TFT arrays were fabricated on the wafer-scale Corning glass and PEN substrates. As shown in Fig.7 (a, b, c), 36 TFTs from a wafer-scale Corning glass substrate were measured to examine the array uniformity, which exhibits marginal variation in electrical performance, with average value of field-effect mobility, SS, Vth at 7.78 cm2/Vs, 270.47 mV/dec, 1.34 V and corresponding normalized standard deviation (σ/average) at 0.262 (Fig.7(a)), 0.176 (Fig.7(b)), 0.381 (Fig.7(c)), respectively. Furthermore, a 10×10 IGZO TFT matrix on PEN substrate (Figure 7(d)) using Parylene-C/AlO_x hybrid passivation was also successfully prepared with a thermal budget under 150 °C. As shown in Fig.7(d), hybrid layer passivated IGZO TFT on the flexible TFT matrix shows the typical transfer characteristics with field-effect mobility of 11.6 cm^2/Vs and SS of 247 mV/dec.

4. Conclusion

In this work, we developed hybrid passivation for IGZO TFTs through a Parylene-C/ALD-AlO_x coating method, which not only avoids the damage on the IGZO channel during ALD process but also improves the bias stability of TFTs. With the hybrid passivation, the IGZO TFT has high performance with saturation mobility of 7.9 cm^2/Vs, ON/OFF ratio of more than 10^7, V_{th} at 2.9 V, and hysteresis window of only 0.73 V which is much smaller than the hysteresis window of 1.46 V for Parylene-C passivated TFT. Compared to the Parylene-C passivated TFT, the hybrid passivation TFT enhances the bias stability from 4.10 V to 1.44 V for the positive stress condition and from -1.26 V to -0.27 V for the negative stress condition. The mechanism of the enhanced stability was explained by extracting electron concentration within the IGZO channel through a Mott-Schottky analysis. A significant electron concentration reduction was found in the Parylene-C passivated IGZO channel from $4.16*10^{21}$ to $2.48*10^{21}$ cm^{-3} after holding 10 V bias stress for 600s while the carrier concentration doesn't vary too much in the IGZO channel covered by hybrid passivation. To further understand the bilayer passivation structure, XRD measurement was conducted where a new peak of the hybrid structure occurs between the peak of Parylene-C and AlO_x, implying a hybrid architecture is formed with a low density of pinholes and voids. We also performed the AFM analysis to confirm that pinholes and 'valleys' at Parylene-C surface have been covered by AlO_x during ALD process and the roughness of the hybrid structure is found to be less than ~4nm. In the end, the uniformity data for mobility, SS and V_{th} was provided from 36 hybrid passivated IGZO TFTs from a wafer-scale array. Meanwhile, we demonstrated a 10×10 IGZO TFT matrix on a PEN substrate using the hybrid passivation method, showing the potential of applying this hybrid passivation technique for the next generation flexible electronics.

Acknowledgements

This work was supported by the European Research Council (ERC Advance No. 340538, Horizon 2020 No. 685758) and EPSRC (EP/P027628/1).

Reference

[1] L. Petti, N. Münzenrieder, C. Vogt, H. Faber, L. Büthe, G. Cantarella, F. Bottacchi, T. D. Anthopoulos, G. Tröster, *Appl. Phys. Rev.* **2016**, *3*, *021303*.

[2] E. Fortunato, P. Barquinha, R. Martins, *Adv. Mater.* **2012**, *24*, *2945*.

[3] E. M. C. Fortunato, L. M. N. Pereira, P. M. C. Barquinha, A. M. Botelho do Rego, G. Goncalves, A. Vilà, J. R. Morante, R. F. P. Martins, *Appl. Phys. Lett.* **2008**, *92*, *222103*.

[4] Y. H. Kim, J. S. Heo, T. H. Kim, S. Park, M. H. Yoon, J. Kim, M. S. Oh, G. R. Yi, Y. Y. Noh, S. K. Park, *Nature.* **2012**, *489*, *128*.

[5] K. K. Banger, Y. Yamashita, K. Mori, R. L. Peterson, T. Leedham, J. Rickard, H. Sirringhaus, *Nat. Mater.* **2011**, *10*, *45*.

[6] H. H. Hsu, C. Y. Chang, C. H. Cheng, P. C. Chen, Y. C. Chiu, P. Chiou, C. P. Cheng, *J. Disp. Technol.* **2014**, *10*, *847*.

[7] T. H. Kim, K. S. Cho, E. K. Lee, S. J. Lee, J. Chae, J. W. Kim, D. H. Kim, J. Y. Kwon, G. Amaratunga, S. Y. Lee, B. L. Choi, Y. Kuk, J. M. Kim, K. Kim, *Nat. Photonics.* **2011**, *5*, *176*.

[8] X. Liu, W. Wu, W. Chen, H. Ning, X. Zhang, W. Yuan, M. Xiong, X. Wang, R. Yao, J. Peng, *Materials.* **2018**, *11*.

[9] H. Xu, D. Luo, M. Li, M. Xu, J. Zou, H. Tao, L. Lan, L. Wang, J. Peng, Y. Cao, *J. Mater. Chem. C.* **2014**, *2*, *1255*.

[10] J. K. Jeong, H. Won Yang, J. H. Jeong, Y. G. Mo, H. D. Kim, *Appl. Phys. Lett.* **2008**, *93*, *123508*.

[11] M. C. Choi, Y. Kim, C. S. Ha, *Prog. Polym. Mater. Sci.* **2008**, *33*, *581*.

[12] J. Wu, Y. Chen, D. Zhou, Z. Hu, H. Xie, C. Dong, *Mater. Sci. Semicond. Process.* **2015**, *29*, *277*.

[13] H. S. Seo, J. U. Bae, D. H. Kim, Y. Park, C. D. Kim, I. B. Kang, I. J. Chung, J. H. Choi, J. M. Myoung, *Electrochem. Solid-State Lett.* **2009**, *12*, *H348*.

[14] D. S. Han, J. H. Park, M. S. Kang, S. R. Shin, Y. J. Jung, D. K. Choi, J. W. Park, *J. Electron. Mater.* **2015**, *44*, *651*.

[15] S. Hong, S. P. Park, Y. G. Kim, B. H. Kang, J. W. Na, H. J. Kim, *Sci. Rep.* **2017**, *7*, *16265*.

[16] D. C. Corsino, J. P. S. Bermundo, M. N. Fujii, K. Takahashi, Y. Ishikawa, Y. Uraoka, *Appl. Phys. Express.* **2018**, *11*.

[17] S. Jeon, S. E. Ahn, I. Song, C. J. Kim, U. I. Chung, E. Lee, I. Yoo, A. Nathan, S. Lee, J. Robertson, K. Kim, *Nat. Mater.* **2012**, *11*, *301*.

[18] T. T. T. Nguyen, B. Aventurier, T. Terlier, J. P. Barnes, F. Templier, *J. Disp. Technol.* **2015**, *11*, *554*.

[19] A. Olziersky, P. Barquinha, A. Viì, L. Pereira, G. Goṇalves, E. Fortunato, R. Martins, J. R. Morante, *J. Appl. Phys.* **2010**, *108*.

[20] S. E. Liu, M. J. Yu, C. Y. Lin, G. T. Ho, C. C. Cheng, C. M. Lai, C. J. Lin, Y. C. King, Y.

H. Yeh, *IEEE Electron Device Lett.* **2011**, *32*, *161*.

[21] M. G. Kim, M. G. Kanatzidis, A. Facchetti, T. J. Marks, *Nat. Mater.* **2011**, *10*, *382*.

[22] H. H. Hsu, Y. C. Chiu, P. Chiou, C. H. Cheng, *J. Alloys Compd.* **2015**, *643*, *S133*.

[23] S. H. Choi, J. H. Jang, J. J. Kim, M. K. Han, *IEEE Electron Device Lett.* **2012**, *33*, *381*.

[24] X. Xu, L. Feng, S. He, Y. Jin, X. Guo, *IEEE Electron Device Lett.* **2012**, *33*, *1420*.

[25] J. Martins, P. Bahubalindruni, A. Rovisco, A. Kiazadeh, R. Martins, E. Fortunato, P. Barquinha, *Materials.* **2017**, *10*, *680*.

[26] A. Kiazadeh, H. L. Gomes, P. Barquinha, J. Martins, A. Rovisco, J. V. Pinto, R. Martins, E. Fortunato, *Appl. Phys. Lett.* **2016**, *109*, *051606*.

[27] J. S. Park, T. W. Kim, D. Stryakhilev, J. S. Lee, S. G. An, Y. S. Pyo, D. B. Lee, Y. G. Mo, D. U. Jin, H. K. Chung, *Appl. Phys. Lett.* **2009**, *95*.

[28] C. L. Fan, M. C. Shang, B. J. Li, Y. Z. Lin, S. J. Wang, W. D. Lee, B. R. Hung, *Materials.* **2015**, *8*, *1704*.

[29] X. Zhou, G. Wang, Y. Shao, L. Zhang, H. Lu, S. Chen, D. Han, Y. Wang, S. Zhang, *SID Int. Symp. Dig. Tech. Pap.* **2017**, *48*.

[30] S. Y. Huang, T. C. Chang, M. C. Chen, S. C. Chen, C. T. Tsai, M. C. Hung, C. H. Tu, C. H. Chen, J. J. Chang, W. L. Liau, *Electrochem. Solid-State Lett.* **2011**, *14*.

[31] Z. Ye, Y. Yuan, H. Xu, Y. Liu, J. Luo, M. Wong, *IEEE Trans. Electron Devices.* **2017**, *64*, *438*.

[32] J. K. Jeong, D. U. Jin, H. S. Shin, H. J. Lee, M. Kim, T. K. Ahn, J. Lee, Y. G. Mo, H. K. Chung, *IEEE Electron Device Lett.* **2007**, *28*, *389*.

[33] K. Gelderman, L. Lee, S. Donne, *J. Chem. Educ.* **2007**, *84*, *685*.

[34] M. Golda-Cepa, K. Engvall, A. Kotarba, *RSC Adv.* **2015**, *5*, *48816*.

[35] P. Bhawal, S. Ganguly, T. K. Chaki, N. C. Das, *RSC Adv.* **2016**, *6*, *20781*.

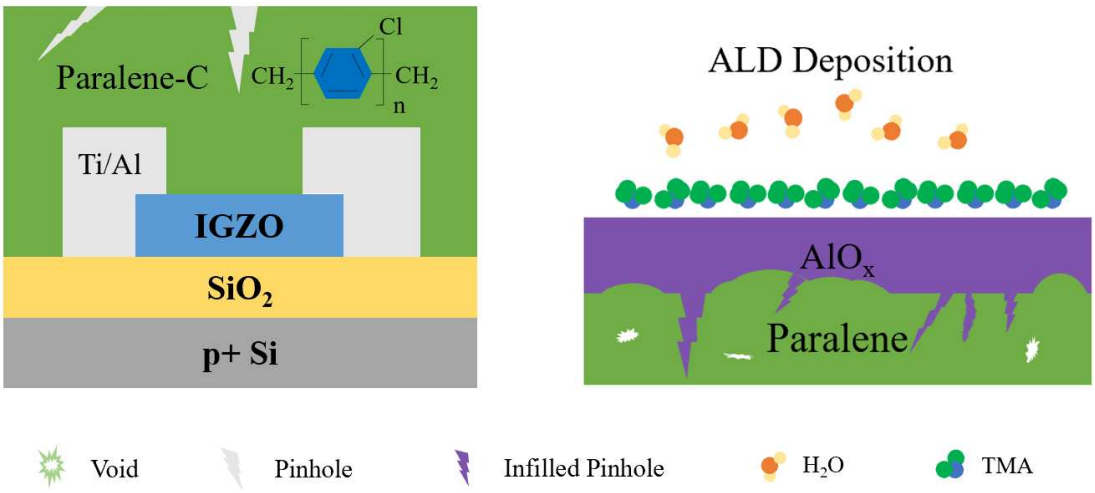

Figure 1. Schematic of Parylene-C passivated IGZO TFT, and the hybrid structure with AlO_x coated on top of Parylene-C by ALD.

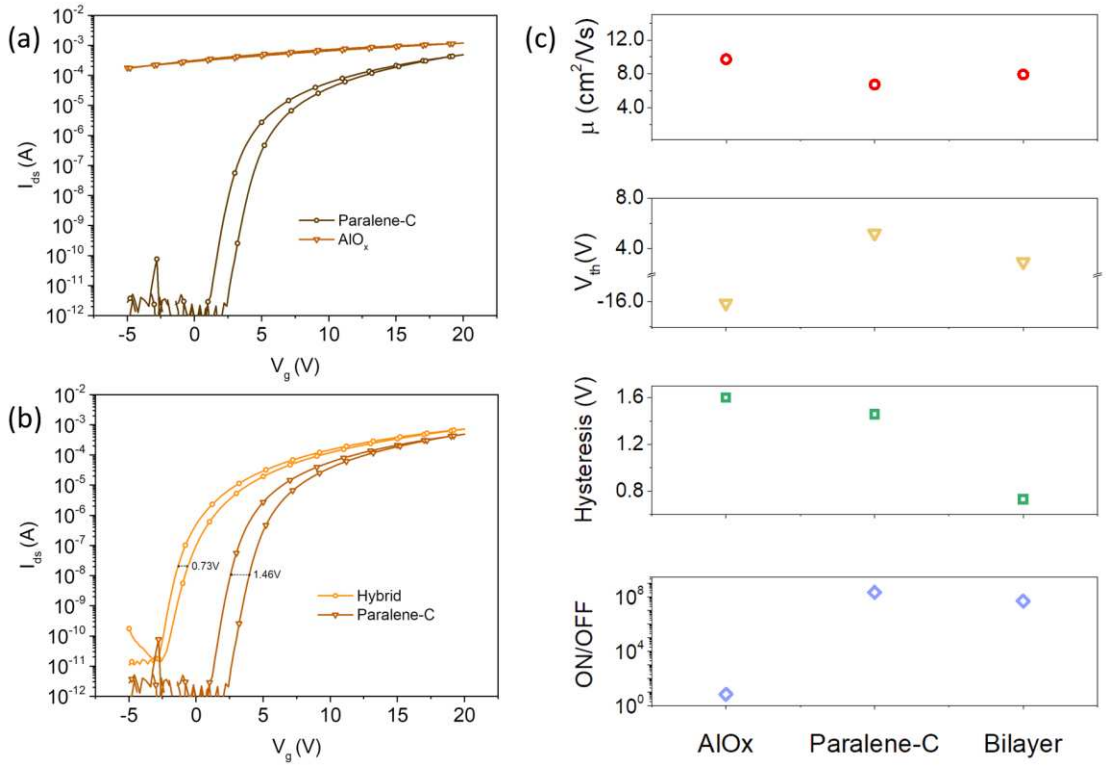

Figure 2. (a) Transfer curves comparison of IGZO TFTs passivated by Parylene-C and AlO_x, (b) Transfer curves comparison of IGZO TFTs passivated by Parylene-C and the hybrid layer, (c) Extracted saturation mobility, V_{th}, hysteresis and ON/OFF ratio for the AlO_x TFT, the Parylene-C passivated TFT and the hybrid layer passivated TFT. All the transfer curves were measured at V_{ds}=20V.

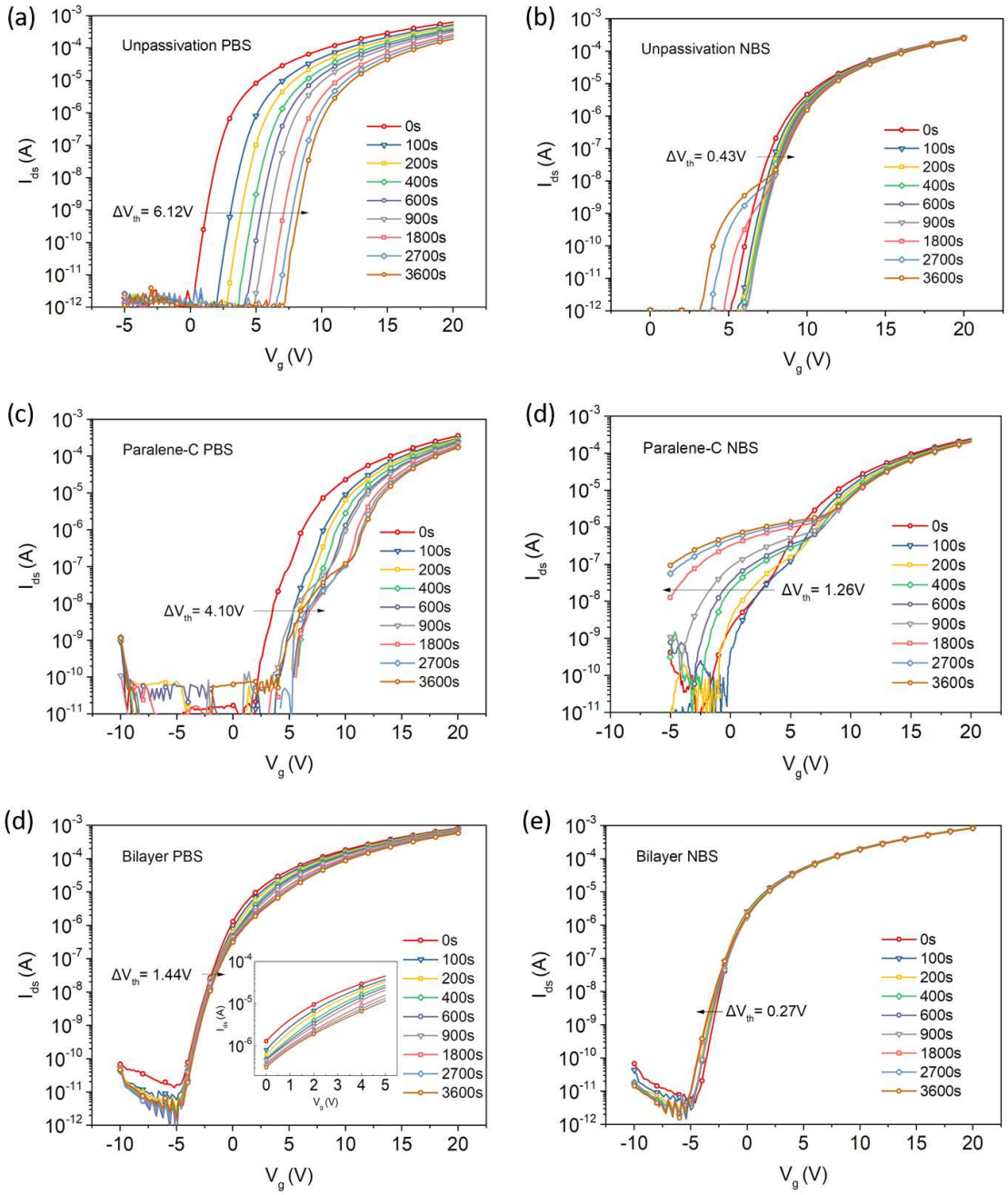

Figure 3. Bias stability test for unpassivated (a)(b), Parylene-C passivated (c)(d) and hybrid layer passivated (e)(f) IGZO TFT under positive bias condition with Vds=20 V, Vgs=10 V (a)(c)(e) and negative bias condition with Vds=20 V, Vgs = -10 V (b)(d)(f).

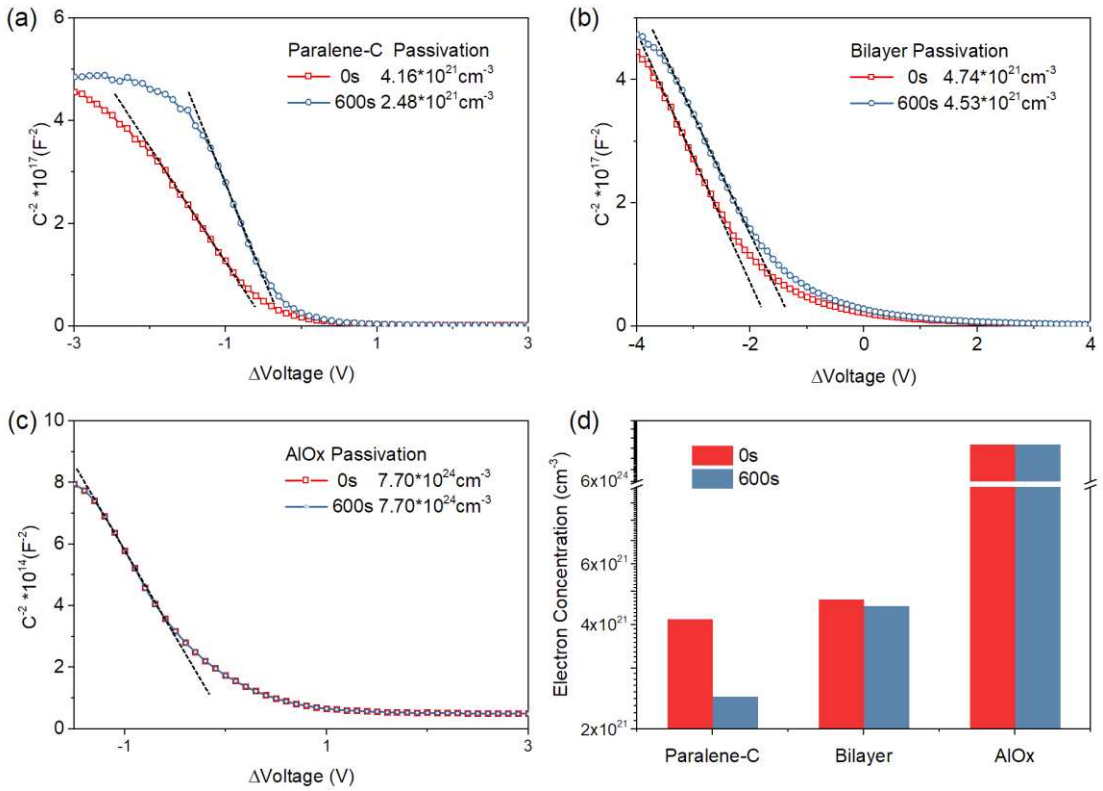

Figure 4. Mott-Schottky analysis for extracting electron concentration of IGZO under the passivation of (a) Parylene-C, (b) Parylene-C/AlO_x hybrids, and (c) AlO_x. Red and blue curves represent the channel electron concentration before and after 600s bias stress (at 10 V). (d) Comparison of electron concentration before and after 600s bias stress for IGZO channels passivated by Parylene-C, hybrids and AlO_x.

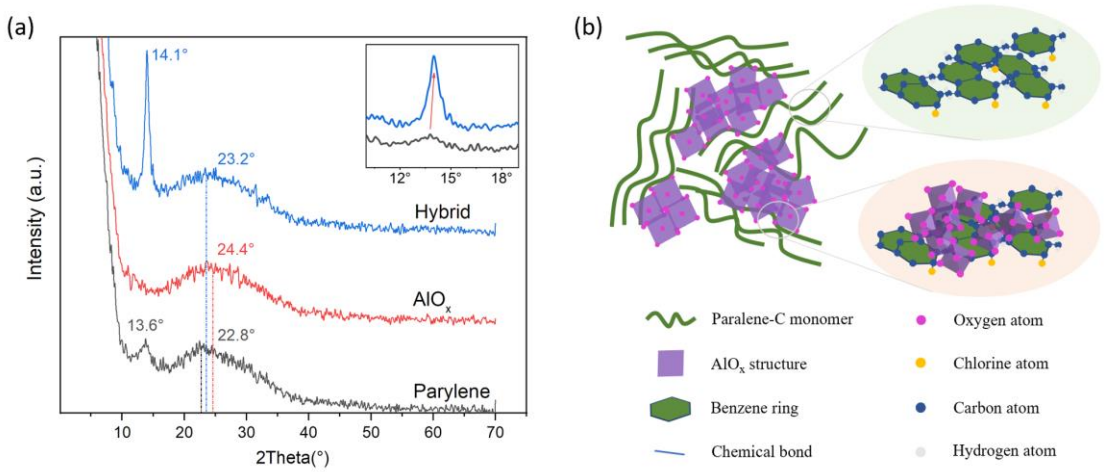

Figure 5. (a) XRD data for 200 nm Parylene-C, 50 nm AlO_x and hybrid film on glass substrates. The inset figure shows the difference between the XRD peak location of the hybrid and Parylene film. (b) Schematic of the hybrid structure formed between Parylene-C and AlO_x.

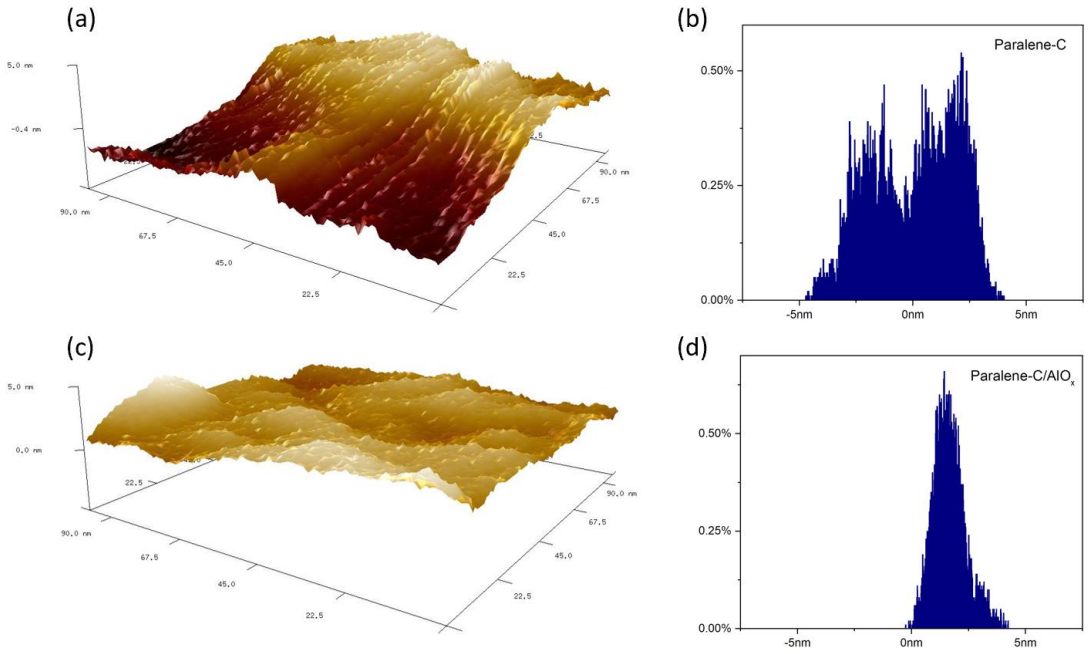

Figure 6. 3D AFM images and surface height distribution for (a)(b) the Parylene-C film on glass and (c)(d) the Parylene-C/AlO_x film on glass. Both AFM images are set to the height range from -5nm to 5nm within 100 nm^2 horizontal area.

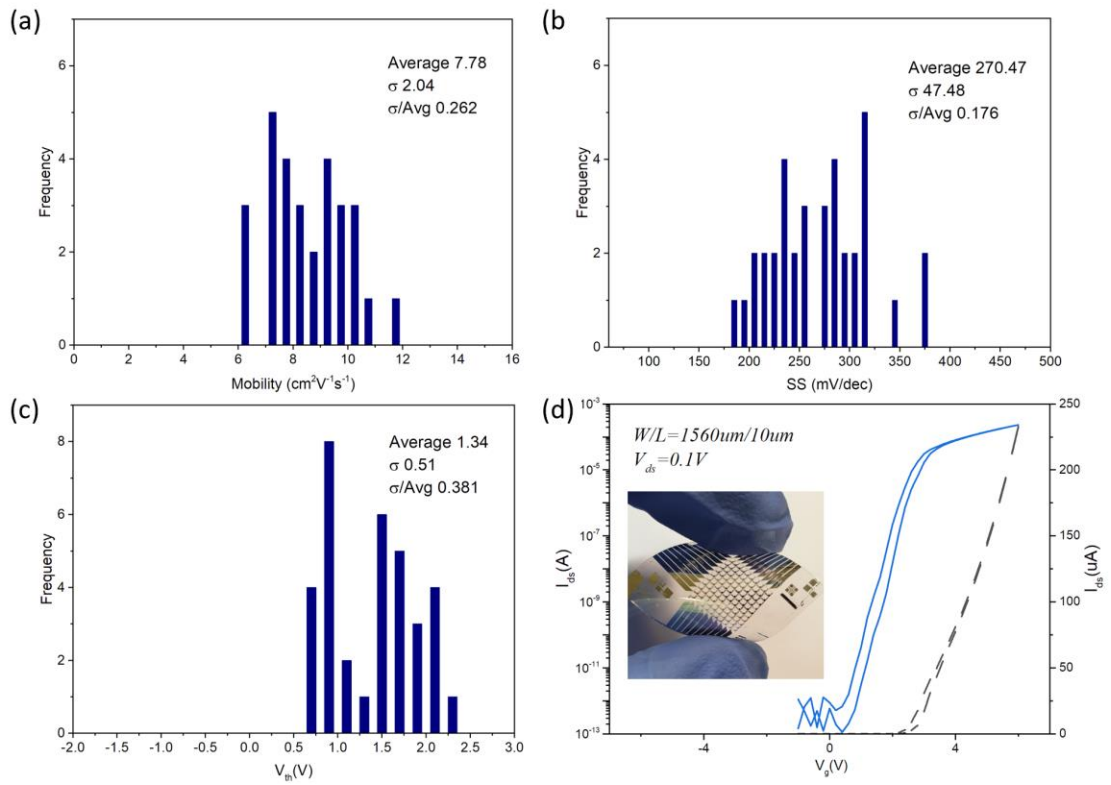

Figure 7. Uniformity histogram for (a) field-effect mobility, (b) SS and (c) V_{th} extracted from TFTs in the matrix. (d) Typical IGZO TFT transfer curve (blue curve in log regime and black curve in linear regime) within a 10×10 TFT matrix with Parylene-C/ALD-AlO_x hybrid passivation on a PEN substrate. Inset figure: The image of a flexible TFT matrix fabricated on a PEN substrate.

Table of content